JACS
JOURNAL OF THE AMERICAN CHEMICAL SOCIETY
Article
pubs.acs.org/JacS

Relaxation Dynamics of Identical Trigonal Bipyramidal Cobalt Molecules with Different Local Symmetries and Packing Arrangements: Magnetostructural Correlations and *ab inito* Calculations

Toby J. Woods,[†,§] María F. Ballesteros-Rivas,[†,⊥] Silvia Gómez-Coca,[†,∥] Eliseo Ruiz,[‡] and Kim R. Dunbar*[,†]

[†]Department of Chemistry, Texas A&M University, College Station, Texas 77842, United States
[‡]Departament de Química Inorgànica i Orgànica and Institut de Recerca en Química Teòrica i Computacional, Universitat de Barcelona, Barcelona 08028, Spain

Supporting Information

ABSTRACT: A family of isostructural, mononuclear Co^{II} complexes with distorted trigonal bipyramidal coordination environments is reported. The degree of distortion as well as the overall symmetry of the molecules varies among the members of the series. Different experimental procedures resulted in the isolation of solvomorphs (pseudopolymorphs with different solvent content) for some of the family members. Importantly, their disparate packing arrangements lead to very different dynamic magnetic behavior. The results of magnetostructural correlations and *ab initio* calculations reveal that the deciding factor for SMM behavior is not the degree of distortion which, *a priori*, would be expected to be the case, but rather the interactions between neighboring molecules in the solid state.

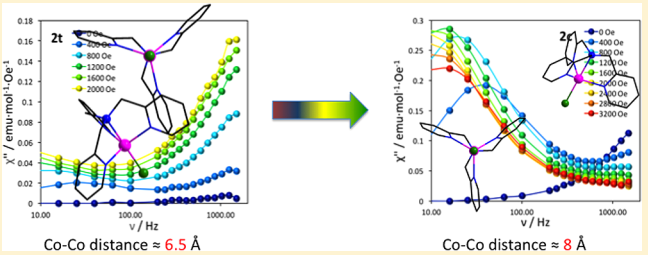

INTRODUCTION

The search for polynuclear compounds that exhibit SMM behavior is a vital research area but, recently, focus has shifted from large spin ground-state molecules to smaller molecules including mononuclear systems. This trend reflects the fact that controlling magnetic anisotropy, which is crucial for determining the energy barrier to spin reversal, is simplified when there is only one spin-bearing metal ion. In fact there are numerous reports in the literature regarding the SMM behavior of complexes containing a single lanthanide ion[1−3] and reports of SMM behavior for mononuclear complexes are increasing rapidly.[4−13] Several mononuclear Fe^{I} and Fe^{II} complexes[14−16] and, very recently, Ni^{I} and Ni^{II} SMMs[17−19] have been reported.

With respect to Co^{II} SMMs, the library of such molecules includes a seven-coordinate pentagonal bipyramidal complex[20] and an eight-coordinate square antiprismatic complex.[21] The highest reported effective energy barrier to date for a mononuclear Co^{II} complex is 230 cm^{-1} for the four-coordinate $(HNEt_3)_2[Co^{II}(L^{2-})_2]$ (H_2L = 1,2-bis(methanesulfonamido)-benzene).[22] Regarding pentacoordinate Co^{II} SMMs, compounds have been reported with geometries ranging from square pyramidal to trigonal bipyramidal,[10−12] including several distorted geometries.[23−25] Compounds with trigonal bipyramidal coordination environments include $[Co(Me_6tren)Cl](ClO_4)$ and $[Co(Me_6tren)Br]Br$,[4] $[Co(Me_6tren)H_2O](NO_3)_2$,[5] $[Co(tbta)N_3](ClO_4)\cdot 3CH_3CN$ (tbta = tris[(1-benzyl-1H-1,2,3-triazol-4-yl)methyl]amine),[26] and $[Co(NS_3^{iPr})Cl](BPh4)$ (NS_3^{iPr} = (2-(isopropylthio)ethyl)-amine)).[27]

Herein we report our efforts to exploit the single-ion anisotropy of Co^{II} in mononuclear complexes that have the potential to be used as secondary building units for heterometallic coordination complexes. The series of mononuclear complexes of general formula $[Co(TPMA)X]^{n+}(Y)_m$ (TPMA = tris(2-pyridylmethyl)amine, X = CH_3CN, n = 2, Y = BF_4, m = 2; X = Cl, Br, and I, n = 1, Y = Cl, Br, and I, m = 1) was synthesized in which the Co^{II} ion resides in a trigonal bipyramidal (TBP) environment with the axial ligand being CH_3CN, Cl^-, Br^-, or I^-. The TPMA group was chosen as the capping ligand to provide a rigid backbone for the cobalt center while leaving one coordination site for further chemistry to occur.

EXPERIMENTAL DETAILS

Syntheses. The TPMA ligand and $[Co(CH_3CN)_6](BF_4)_2$ were prepared by literature procedures[28,29] The starting materials $CoCl_2$ (Strem), $CoCl_2\cdot 6H_2O$ (Fisher Scientific), $CoBr_2$ (Alfa Aesar), and CoI_2 (Alfa Aesar) were used as received. The hydrate $CoBr_2\cdot 6H_2O$ was prepared under ambient air conditions by dissolving anhydrous

Received: September 27, 2016
Published: November 10, 2016

DOI: 10.1021/jacs.6b10154
J. Am. Chem. Soc. 2016, 138, 16407−16416

$CoBr_2$ in distilled H_2O followed by evaporation to produce a microcrystalline pink-red solid.

The syntheses of $[Co(TPMA)CH_3CN](BF_4)_2$, the cubic phases of [Co(TPMA)Cl]Cl and [Co(TPMA)Br]Br, and [Co(TPMA)I]I were performed in an MBRAUN drybox under an N_2 atmosphere. CH_3CN was predried by storage over 3 Å molecular sieves, distilled from 3 Å molecular sieves, and stored over 3 Å molecular sieves in the drybox. Et_2O was purified using an MBRAUN solvent purification system and then stored over 3 Å molecular sieves in the drybox. Toluene was purified using an MBRAUN solvent purification system and then stored over 3 Å molecular sieves in the drybox. Synthesis of the triclinic phases of [Co(TPMA)Cl]Cl and [Co(TPMA)Br]Br were performed under ambient air conditions using ACS-grade solvents that were used as received without further purification.

*[Co(TPMA) $(CH_3CN)](BF_4)_2\cdot CH_3CN$ (**1**).* Samples of TPMA (0.0290 g, 0.0999 mmol) and $[Co(CH_3CN)_6][BF_4]_2$ (0.0478 g, 0.0998 mmol) were placed in a vial, and 5 mL of CH_3CN was added. The resulting red solution was stirred for 24 h and filtered. Red X-ray quality crystals were obtained by slow diffusion of Et_2O vapor into the filtrate. Yield: 0.0493 g (82%). Analysis calculated (found) for $[Co(TPMA)(CH_3CN)](BF_4)_2\cdot CH_3CN$ ($C_{22}H_{24}N_6B_2F_8Co$): C: 43.68% (43.55%), H: 4.00% (3.95%), N: 13.89% (13.68%).

*[Co(TPMA)Cl]Cl·2.4H_2O Triclinic Phase (**2t**).* The triclinic phase of [Co(TPMA)Cl]Cl was prepared by a literature procedure.[30] A redetermination of the crystal structure in conjunction with TGA and IR analysis revealed that the salt as isolated in the present case is not anhydrous as reported. The TPMA ligand (0.0949 g, 0.327 mmol) was dissolved in 4.2 mL of MeOH to give a colorless solution that was then added to solid $CoCl_2\cdot 6H_2O$ (0.0787 g, 0.331 mmol), which produced a green solution. After stirring for 1 h, the MeOH was evaporated to yield a green residue, which was dissolved in a minimum volume of CH_2Cl_2 (~15 mL). Gravity filtration through Whatman filter paper was performed to remove a small quantity of brown solid. Bulk green X-ray quality crystals were obtained by layering the dark green filtrate with Et_2O. The stated water content in the formula is an average of the water content indicated by elemental analysis and TGA. Yield: 0.0892 g (59%). Analysis calculated (found) for [Co(TPMA)-Cl]Cl·2.7H_2O ($C_{18}H_{23.4}N_4Cl_2O_{2.7}Co$): C 46.11% (46.06%), H 5.03% (4.92%), N 11.95% (11.96%).

*[Co(TPMA)Cl]Cl Cubic Phase (**2c**).* Quantities of $CoCl_2$ (0.0333 g, 0.256 mmol) and TPMA (0.0761 g, 0.262 mmol) were dissolved in 6.0 mL of CH_3CN in a vial. The resulting green solution was stirred for 24 h and then filtered. Bulk green X-ray quality crystals were obtained by layering the green filtrate over toluene. Yield: 0.0401 g (37%). Analysis calculated (found) for [Co(TPMA)Cl]Cl ($C_{18}H_{18}N_4Cl_2Co$): C 51.45% (50.96%), H 4.32% (4.38%), N 13.33% (13.27%).

*[Co(TPMA)Br]Br·2.0H_2O Triclinic Phase (**3t**).* The triclinic phase of [Co(TPMA)Br]Br was prepared by substituting $CoBr_2\cdot 6H_2O$ for $CoCl_2\cdot 6H_2O$ in the reported synthesis for the triclinic phase of [Co(TPMA)Cl]Cl.[30] TPMA (0.0758 g, 0.261 mmol) was dissolved in 5.2 mL of MeOH to give a colorless solution that was added to solid $CoBr_2\cdot 6H_2O$ (0.0825 g, 0.252 mmol) to give a blue solution. After being stirred for 1 h, the MeOH was evaporated to produce a dark blue-green residue, which was dissolved in the minimum amount of CH_2Cl_2 (~15 mL) to give a dark blue-green solution. The solution was gravity filtered through Whatman filter paper to remove a small quantity of brown solid. Green crystals were obtained by layering the blue-green solution with Et_2O. These crystals were highly twinned and unsuitable for X-ray structural determination. The product was recrystallized by layering Et_2O on a solution of the crystals in 10 mL of CH_2Cl_2, which yielded a bulk quantity of X-ray quality crystals. The water content in the formula is reported as an average of the water content obtained by elemental analysis and TGA. Recrystallized yield: 0.066 g (47%). Analysis calculated (found) for [Co(TPMA)Br]Br·2.7H_2O ($C_{18}H_{23.4}N_4Br_2O_{2.7}Co$): C 38.83% (39.07%), H 4.22% (3.98%), N 10.06% (9.81%).

*[Co(TPMA)Br]Br Cubic Phase (**3c**).* $CoBr_2$ (0.0436 g, 0.199 mmol) and TPMA (0.0540 g, 0.186 mmol) were placed in a vial and treated with 5 mL of CH_3CN. The resulting blue-green solution was stirred for 24 h and then filtered through a fine porosity glass frit. Green X-ray quality crystals were obtained by layering the blue filtrate with Et_2O. Yield: 0.0418 g (44%). Analysis calculated (found) for [Co(TPMA)-Br]Br ($C_{18}H_{18}N_4Br_2Co$): C 42.47% (42.73%), H 3.56% (3.66%), N 11.00% (10.93%).

*[Co(TPMA)I]I (**4**).* CoI_2 (0.0311 g, 0.0994 mmol) and TPMA (0.0290 g, 0.0999 mmol) were placed in a vial and dissolved in 5 mL of CH_3CN. The resulting blue-purple solution was stirred for 24 h after which time the solution was filtered through a fine porosity glass frit. Pink-purple X-ray quality crystals were obtained by layering the blue-purple filtrate with Et_2O. Yield: 0.0239 g (40%). Analysis calculated (found) for [Co(TPMA)I]I ($C_{18}H_{18}N_4I_2Co$): C 35.85% (36.10%), H 3.01% (3.06%), N 9.29% (9.18%).

X-ray Crystallographic Studies. Single-crystal X-ray data for $[Co(TPMA)(CH_3CN)](BF_4)_2$, [Co(TPMA)Cl]Cl (triclinic phase), [Co(TPMA)Cl]Cl (cubic phase), [Co(TPMA)Br]Br (cubic phase), and [Co(TPMA)I]I were collected on a Bruker APEXII (Mo Kα) diffractometer equipped with a CCD detector. Suitable crystals were affixed to either a nylon loop or a MiTeGen MicroLoop with Paratone oil and placed in a cold stream of N_2(g) at 110 K for all crystals except [Co(TPMA)I]I, which was collected at 150 K. The triclinic phase of [Co(TPMA)Br]Br was collected on a Bruker D8 Venture (Cu Kα Iμs microfocus) instrument equipped with a CMOS detector. A suitable crystal was affixed to a MiTeGen MicroLoop with Paratone oil and placed in a cold stream of N_2(g) at 100 K. For all structures, the frames were integrated with the Bruker APEXII software package,[31] and a semiempirical absorption correction was applied using SADABS as contained within the Bruker APEXII software suite. The structure was solved using SHELXT[32] and refined using SHELXL-2014[33] as implemented in ShelXle, a graphical interface for the SHELX suite of programs.[34] The remaining nonhydrogen atoms were located by alternating cycles of least-squares refinements and difference Fourier maps. All hydrogen atoms were placed in calculated positions with the exception of the water hydrogen atoms in the triclinic phases of [Co(TPMA)Cl]Cl and [Co(TPMA)Br]Br which were not assigned. The final refinements were carried out with anisotropic thermal parameters for all non-hydrogen atoms. Crystals of [Co(TPMA)I]I were invariably found to be nonmerohedral twins. The crystal chosen for the structural study was refined as a two-domain twin with the twin fractions refining to 40.3 and 59.7%.

The outer-sphere halide ions in the triclinic phases of [Co(TPMA)-Cl]Cl and [Co(TPMA)Br]Br are disordered over multiple positions, as are the water molecules. The positions and site occupancy of the outer-sphere halide ions and water oxygen atoms of the triclinic phase of [Co(TPMA)Cl]Cl were refined as follows. One outer-sphere Cl^- could be assigned definitively. None of the remaining electron density peaks were of sufficient intensity to warrant assignment as a fully occupied chloride ion. TGA and IR analysis indicated that at least some of the residual electron density was due to the presence of water molecules. The refinement was conducted on the premise that any residual electron density peak of intensity greater than $8e^-/Å^3$ was unlikely to be water. These peaks were assigned as partially occupied Cl^- ions. A site occupancy constraint was used to constrain the total occupancy of the disordered Cl^- such that the total occupancy of the unit cell was 12, the value required to balance the charge of the six Co^{II} ions in the unit cell. The highest remaining residual density peaks were assigned as partially occupied Cl^- ions until the thermal parameters reached reasonable values. This strategy resulted in three positions being assigned as disordered Cl^- with site occupancies of 78.8, 52.7, and 68.3%. The remaining residual density peaks were then assigned as H_2O oxygen atoms using a methodology similar to that used for the Cl^- ions. A constraint was used to constrain the site occupancy of the disordered oxygen atoms such that the total H_2O oxygen occupancy of the unit cell was 12, resulting in a molecular formula of [Co(TPMA)-Cl]Cl·2H_2O. A total of 12 oxygen atoms from H_2O were assigned with occupancies ranging from 25.3 to 75.1%. Attempts to refine the water oxygen occupancy of the unit cell to the fractional molecular content observed by TGA and elemental analysis resulted in convergence problems. While the structure refines well in this manner, there is no way to be certain that all of the disordered Cl^- and H_2O molecules are assigned to the correct positions. For example, the Cl^- ion occupied at

DOI: 10.1021/jacs.6b10154
J. Am. Chem. Soc. 2016, 138, 16407−16416

52.3% could be a fully occupied H_2O oxygen atom. Additionally, it is possible that some of the assigned positions are partially occupied as Cl^- and partially occupied as H_2O. While this model is not ideal, it is a better description of the reality of the system than the structure published in the literature[30] in which no H_2O molecules were assigned. The unit cell determined in this work and the literature are the same, consistent with the same compound being formed. The authors of the literature procedure for this compound report no elemental analysis, IR data, or TGA results to support their assignment of the structure as anhydrous [Co(TPMA)Cl]Cl although they observed similarly disordered, partially occupied chloride ions in their single-crystal structure refinement. The refinement of the outer sphere bromide ions and water oxygen atoms in the triclinic phase of [Co(TPMA)Br]Br was carried out in a similar manner. Cambridge Crystallographic Database Centre numbers are as follows: 1011895 ([Co(TPMA)-CH_3CN]$(BF_4)_2$, 1489343 ([Co(TPMA)Cl]Cl·2.4H_2O triclinic phase), 1429142 ([Co(TPMA)Cl]Cl cubic phase), 1489344 ([Co-(TPMA)Br]Br·2H_2O triclinic phase), 1429144 ([Co(TPMA)Br]Br cubic phase), 1429143 ([Co(TPMA)I]I). Further pertinent details of the X-ray refinements are given in Table S1.

For [Co(TPMA)Cl]Cl, [Co(TPMA)Br]Br, and [Co(TPMA)I]I powder X-ray diffraction experiments were conducted on a Bruker D8-Focus ECO (Cu Kα) Bragg−Brentano diffractometer at room temperature using a silicon zero-background sample holder to verify the phase purity of the bulk sample.

RESULTS AND DISCUSSION

The six salts, [Co(TPMA) $(CH_3CN)](BF_4)_2$·CH_3CN (**1**), [Co(TPMA)Cl]Cl·2.4H_2O (**2t**), [Co(TPMA)Cl]Cl (**2c**), [Co-(TPMA)Br]Br·2H_2O (**3t**), [Co(TPMA)Br]Br (**3c**), and [Co-(TPMA)I]I (**4**), were synthesized by reactions of TPMA with a suitable Co^{II} precursor. Compound **1** crystallizes in the monoclinic space group $P2_1/c$, **2c** and **3c** crystallize in the cubic space group $P2_13$, and **2t**, **3t**, and **4** crystallize in the triclinic space group $P\bar{1}$. For **2t** and **3t**, the water content is an average of the water content as determined by thermogravimetric and elemental analyses. The asymmetric unit of **1**, **2c**, and **3c** contain one crystallographically independent molecule whereas **4** contains two. Compounds **2t** and **3t** contain three crystallographically independent molecules. Details of the X-ray structural refinements are contained in the Experimental Details and Supporting Information.

The coordination sphere of the Co^{II} ions in all of the complexes consists of four nitrogen atoms from the TPMA capping ligand and either one nitrogen atom from a coordinated CH_3CN molecule or a coordinated halide ion. The Shape program,[35,36] which compares the coordination geometry of a molecule to a perfect coordination environment, was used to evaluate the members of this family and it was found that they are best described as trigonal bipyramidal molecules with the equatorial plane defined by the three pyridine N atoms of TPMA with the Co ion being situated slightly below this N3 plane (Figure 1). The Shape value (S) with respect to the TBP geometry (Table S3) was found to vary between 0.97 for **1** and 3.24 for **4** (S is equal to 0 for a perfect TBP geometry). The increase in the S value when descending the halide series is principally due to the increase in the Co−X distance. The cations exhibit approximate C_3 symmetry, with the cubic phases (**2c** and **3c**) having crystallographically imposed C_3 symmetry. As can be seen in Figure 2, if only the first coordination sphere is considered, then the molecules possess C_{3v} symmetry. The mirror plane symmetry is broken by the slight tilt of the pyridine rings and nonplanarity between the methyl carbon atom connecting the pyridine rings to the bridgehead amine nitrogen atom and the pyridine rings themselves.

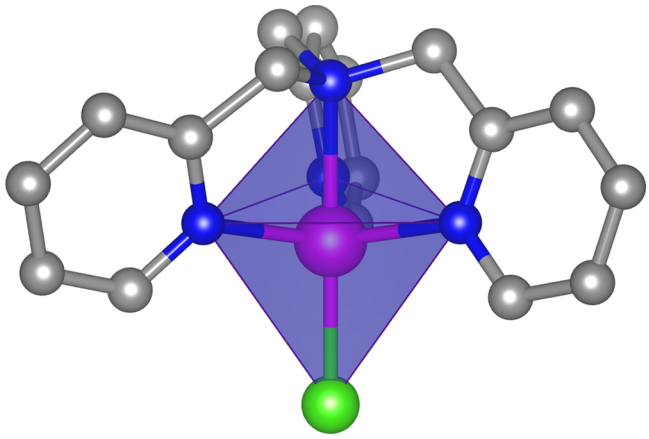

Figure 1. Molecular structure of compound **2c** emphasizing the trigonal bipyramidal geometry (purple polyhedra) with the equatorial plane defined by the three pyridine N atoms of TPMA. Cobalt, chlorine, nitrogen, and carbon are in pink, green, blue, and gray, respectively. Hydrogen atoms have been omitted for the sake of clarity.

For complexes **1**−**4**, the Co^{II} ion projects out of the N_3 plane formed by the TPMA pyridine rings toward the terminal halide or CH_3CN ligand, resulting in N_{py}−Co−N_{amine} angles of less than 90°. This distortion also leads to deviations in the equatorial bond angles from 120°. A list of pertinent bond distances and angles is compiled in Table S2.

For the triclinic phases of [Co(TPMA)Cl]Cl and [Co-(TPMA)Br]Br, **2t** and **3t** respectively, outer-sphere halide and water oxygen atoms are disordered over multiple positions. Details of the methods used to refine the site occupancy of the halide and water oxygen atoms can be found in the Experimental Details section. Powder X-ray diffraction (Figures S1−S3) was used to verify the phase purity of each bulk sample prior to conducting magnetic measurements.

DC Magnetic Measurements. Static DC magnetic measurements were performed on crushed single crystals of **1**−**4** from 1.8 to 300 K (Figure 3). The DC behavior is similar for all six compounds. At 300 K, the χT value is ∼2.4 emu K mol^{-1}, higher than the 1.875 emu K mol^{-1} expected for an S = 3/2 system with g = 2, an indication of single-ion anisotropy due to the Co^{II} ion.

Additionally, M versus H measurements at 1.8 K did not saturate at the highest available field of 7 T, a further indication of a high degree of anisotropy for these systems. Reduced magnetization data for **1**−**4** were recorded between 1.8 and 4 K (Figures S6−S11). The results of fitting the field-dependent magnetization data using PHI[37] are shown in Table 1, along with the results of *ab initio* calculations (*vida infra*).

For **1**, attempts to fit the field-dependent magnetization data with negative values of D resulted in lower-quality fits of the data than did a positive D value; the small value of the transverse anisotropy parameter E is appropriate for a molecule of C_3 symmetry.[4] For **2**− **4**, the fits to the magnetization data are consistent with negative D values. For **2c**, the sign and magnitude of D as well as the g value are in accord with the ZFS parameters derived from EPR studies of [Co(Me_6tren)Cl]-(ClO_4) which crystallizes in the trigonal space group $R3c$.[4] As expected the D value is smaller than the one reported for [Co(NS_3^{iPr})Cl](BPh_4) due to its longer equatorial Co−S distances and, hence, weaker equatorial σ-donation.[27] The

DOI: 10.1021/jacs.6b10154
J. Am. Chem. Soc. 2016, 138, 16407−16416

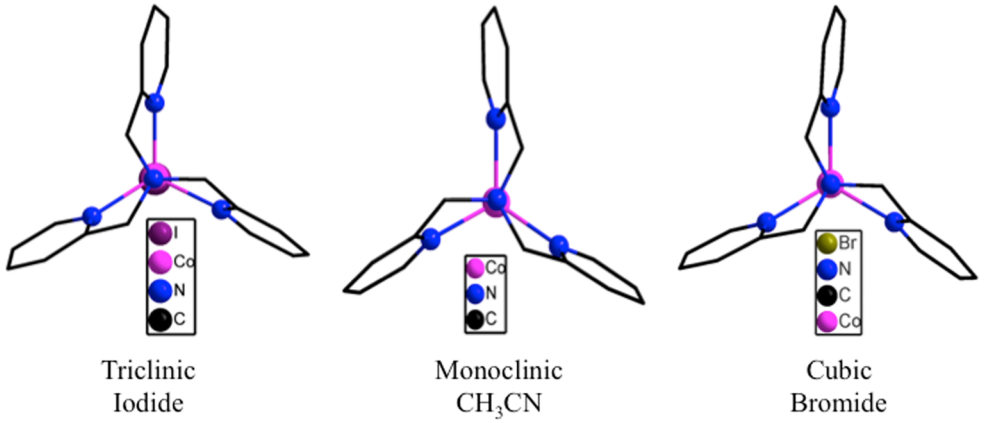

Figure 2. View down the C_3 axis of representative members of the $[Co(TPMA)X]^{1+/2+}$ series.

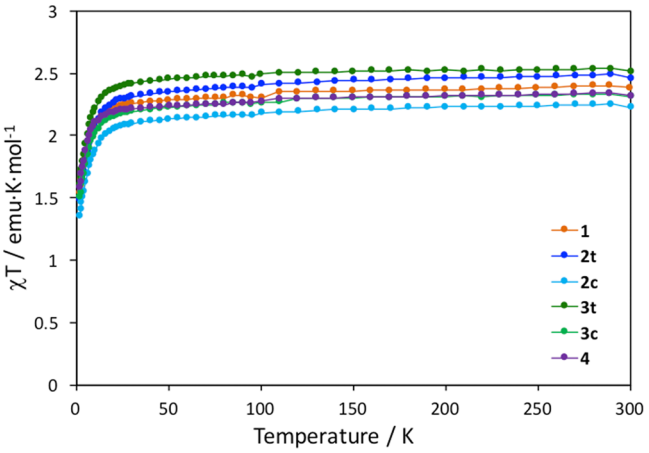

Figure 3. Plot of χT versus T under a 1000 Oe applied field for compounds **1**–**4**.

Table 1. Experimental (PHI) and Calculated (CASSCF+spin orbit) ZFS Parameters (cm^{-1}) and *g* Values for Compounds 1–4

	experimental			calculated		
compound	D	E	g_{iso}	D	$\|E\|$	g_{iso}
1	9.66	0.26	2.39	8.86	0.98	2.23
2t	−6.95	−1.78	2.25	−7.47	0.42	2.26
2c	−8.49	0.0	2.30	−8.63	0.0	2.27
3t	−6.30	1.59	2.34	−4.83	0.41	2.27
3c	−7.18	0.0	2.23	−5.30	0.0	2.27
4	−7.53	1.00	2.37	−2.97	0.66	2.27

similarity in the ZFS parameters between the triclinic and cubic phases **2t** and **2c** suggests that the electronic environment is not significantly affected by the pseudo- C_3 symmetry of the triclinic phase versus the rigorous C_3 symmetry of the cubic phase, except for its influence in the transverse ZFS parameter (E) which is zero in the case of the rigorous C_3 symmetry of the cubic phase. As expected for **3c**, the sign of D is consistent with that reported for $[Co(Me_6tren)Br]Br$ as derived from EPR studies[4] but is larger in magnitude, namely, −2.4 cm^{-1}, for $[Co(Me_6tren)Br]Br$ as compared to −7.2 cm^{-1} for **3c**. The smaller D value for $[Co(Me_6tren)Br]Br$ as compared to $[Co(Me_6tren)Cl]^+$ was attributed to a stronger σ-donor effect from the equatorial amine nitrogen atoms of Me_6tren as evidenced by shortened $Co-N_{amine}$ bond lengths. The authors provided computational evidence that this increase in σ-donation has the effect of increasing the energy gap between the (d_{xz}, d_{yz}) and (d_{xy}, $d_{x^2-y^2}$) orbital sets (Figure 4), leading to

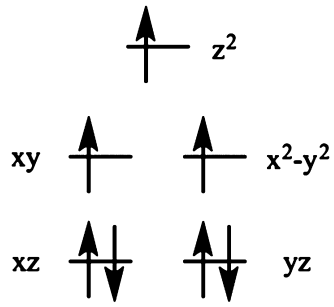

Figure 4. Schematic splitting of the d orbitals for a mononuclear Co^{II} compound in a trigonal bipyramidal geometry.

a smaller D value. The TPMA ligand is more rigid than Me_6tren as evidenced by only minor changes in the Co−TPMA bonding metrics among all members of the family, the consequence of which is that the energy gap between the (d_{xz}, d_{yz}) and (d_{xy}, $d_{x^2-y^2}$) orbital sets remain relatively constant across the series leading to similar D values. As in the case of the chloride analogs, the ZFS parameters for the triclinic bromide phase **3t** are quite close to those obtained for the cubic phase **3c**, being that E is equal to zero for the rigorous C_3 symmetry of the cubic phase. For **4**, fits of similar quality to the reported negative D value could be obtained with a positive D value of similar magnitude and a slightly lower g value. We have chosen to report the negative D value based on the results of the *ab initio* calculations.

AC Magnetic Measurements. Dynamic AC magnetic measurements for **1**–**4** were performed as a function of applied DC field (Figure 5). The optimal DC field was chosen as the field at which a well-resolved maximum in χ'' is visible at 1.8 K. For **2c**, the additional, higher DC fields at which full AC measurements were performed were selected based on the observed differences in AC behavior in the preliminary measurements. A large separation between the applied fields was useful for identifying possible field-dependent relaxation effects. Only compound **2c** exhibits an out-of-phase signal without an applied field in the form of a tail at higher frequencies with no maximum in χ'' being observed. Compounds **2t**, **3t**, and **4** exhibit a nonzero signal in χ'' at high frequencies, but no maximum in the out-of-phase

DOI: 10.1021/jacs.6b10154
J. Am. Chem. Soc. 2016, 138, 16407−16416

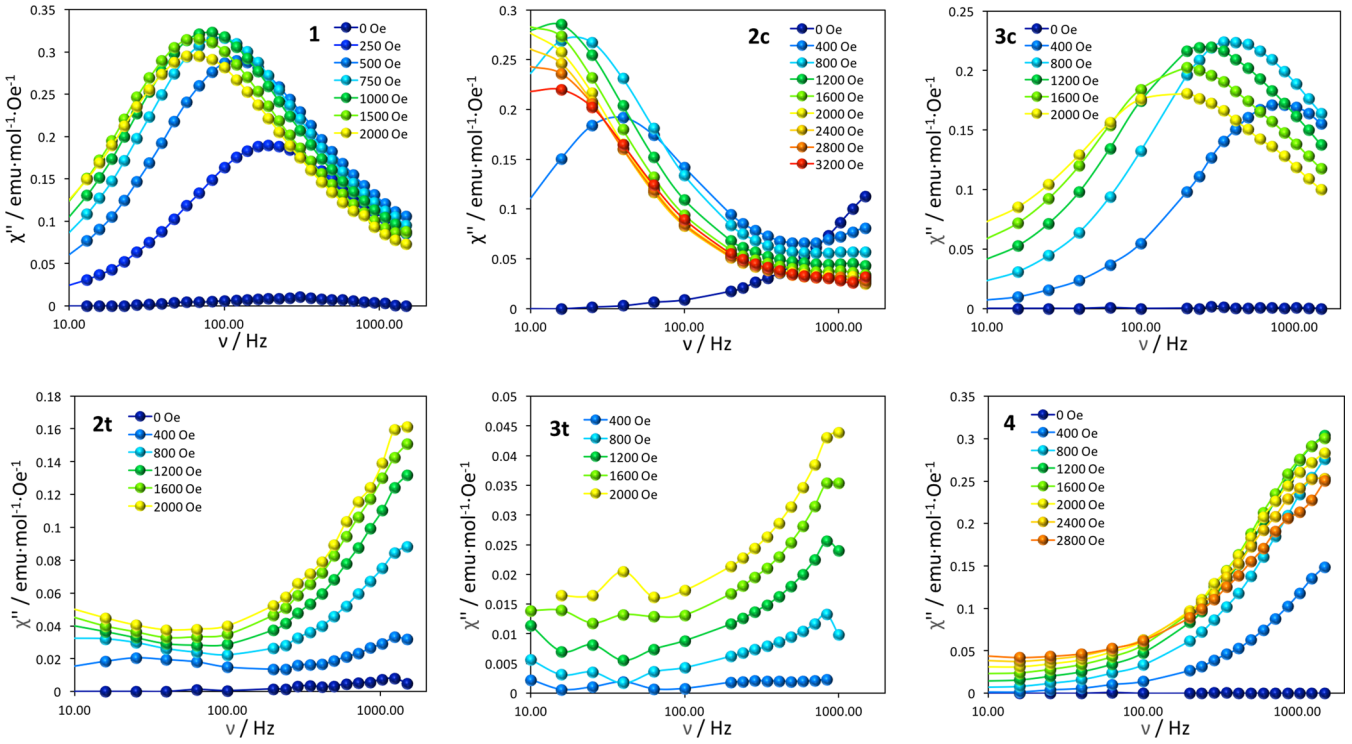

Figure 5. Magnetic data (AC) for **1**−**4** at 1.8 K and different applied DC magnetic fields.

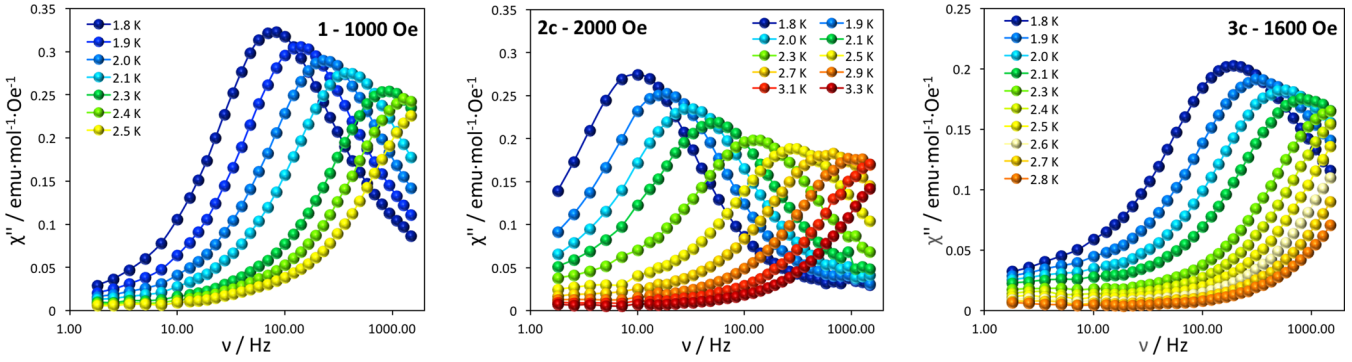

Figure 6. Magnetic data (AC) for **1**, **2c**, and **3c** at different temperatures and applied DC magnetic fields.

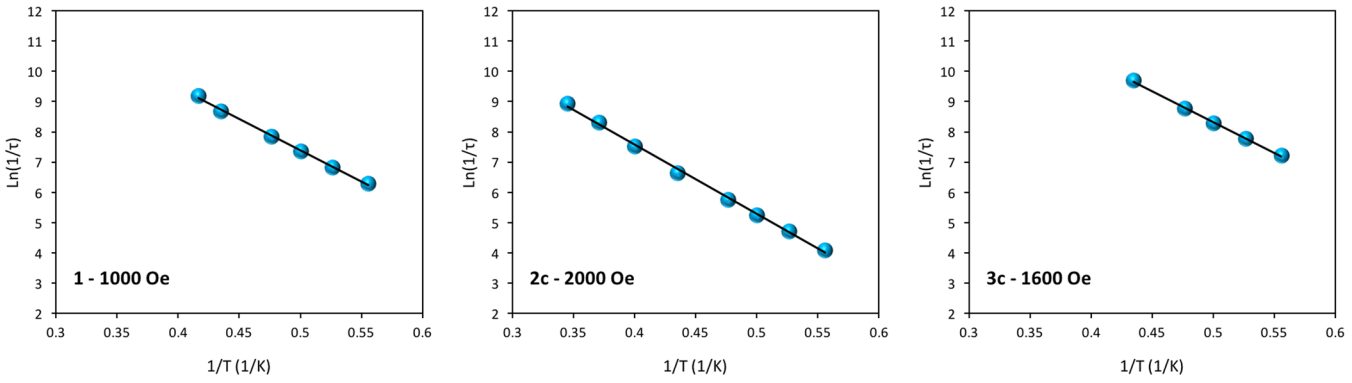

Figure 7. Arrhenius plots for **1**, **2c**, and **3c** at different applied DC magnetic fields. The black line is the fit to the Arrhenius equation.

component was observed. Compounds **1**, **2c**, and **3c**, however, revealed obvious SMM behavior in the presence of an applied dc field. Compound **2c** exhibits a maximum at the lowest frequency (∼20 Hz), followed by compound **1** with a maximum at ∼90 Hz. For **3c** the maximum is only observed at frequencies higher than 100 Hz. The fitting of the Cole−Cole plots for **1**, **2c**, and **3c** using a modified Debye function[38,39] was performed, allowing for the extraction of the τ and α parameters (Figures S12−S15 and Tables S4−S7). For **2c** there is also a distinct tail at high frequencies indicative of a

DOI: 10.1021/jacs.6b10154
J. Am. Chem. Soc. 2016, 138, 16407−16416

second relaxation process. In this case, the fitting of the Cole−Cole plot was performed using only the frequencies from 10 to 415 Hz and by using two relaxation processes. Both procedures lead to nearly identical parameters for the predominant process at lower frequencies. The fitting of τ versus field at 1.8 K with an equation including direct and tunneling relaxation processes and a constant to include the processes with no field dependence is provided in eq S1, Figures S16−S18, and Table S8. For the optimum field, the value of τ^{-1} is predominantly described by the constant parameter. At lower fields, the decrease of τ^{-1} with field can be ascribed to tunneling. For **2c**, the increase of τ^{-1} at higher fields is attributed to a direct process.

In an applied DC field of 1000 Oe, frequency-dependent maxima in χ'' were observed below 2.4 K for **1** (Figure 6). A fitting of the Cole−Cole plot using a modified Debye function[38,39] allowed for the extraction of the τ and α parameters (Figure S19 and Table S9). The τ values were used to construct an Arrhenius plot (Figure 6), from which the relaxation parameters of U_{eff}/k_b = 15 cm^{-1} and $\tau_0 = 1.7 \times 10^{-8}$ s were extracted (Figure 7). The barrier to thermal relaxation in **1** is slightly higher than the 13 cm^{-1} barrier reported for $[Co(Me_6tren)(OH_2)]^{2+}$ with $\tau_0 = 9.6 \times 10^{-9}$ s.[5] The α parameter in **1** varies between 0.14 and 0.16, which is indicative of a relatively narrow distribution of relaxation times.

What is most intriguing about this complex, however, is that there is no evidence of a crossover to a quantum tunneling regime at low temperatures. Among the previously reported mononuclear Co^{II} SMMs, the observation of a tunneling regime at low temperatures is much more common than the observation of thermal spin relaxation down to the lowest measured temperature.[5−9,40−50] Application of a 1000 Oe DC bias field appears to be sufficient for blocking the tunneling pathway at all temperatures above 1.8 K. Since the splitting between the $M_s = \pm^1/_2$ and $\pm^3/_2$ sublevels is 2|*D*| in this case, a purely thermal relaxation pathway should lead to an energy barrier of 20 cm^{-1}, only slightly higher than the observed U_{eff}/k_b of 15 cm^{-1}. This fact further supports the conclusion that tunneling is not a major relaxation pathway above 1.8 K. To further verify the dominance of the Orbach mechanism over other processes, a fit including tunneling, direct, and Raman processes was performed (eq S2). To avoid overparameterization of the fitting, the tunneling and direct parameters were fixed to those previously obtained from the fit of the dependence of τ^{-1} with field. The fit shows a clear dominance of the Orbach process with a small contribution from tunneling (Figure S29 and Table S15) giving U_{eff}/k_b = 17 cm^{-1}, slightly closer to the expected value of 20 cm^{-1}.

Previous reports of Co^{II} SMMs with a large rhombic term have led to the hypothesis that slow relaxation is due to the rhombic term establishing an "easy axis" within the easy plane.[51,52] As the rhombic term is very small in **1** this is not a viable explanation for the SMM behavior in this case. A pseudotetrahedral mononuclear Co^{II} complex with a positive *D* value and a low *E* value reported by Long and co-workers displays SMM behavior in which thermal relaxation was observed instead of direct tunneling between the $M_s = \pm^1/_2$ states; these results were attributed to a phonon bottleneck effect, *viz.*, there are not enough phonon modes of the proper frequency to allow for tunneling to occur.[44] A more recent report from the Ruiz and Luis groups has demonstrated that the inclusion of the hyperfine coupling ($I = {}^7/_2$ for Co) and the nuclear spin−lattice interaction is necessary to explain the spin relaxation in Co^{II} systems with easy-plane anisotropy.[53]

For compound **2c** in a 400 Oe DC field, there are frequency-dependent maxima in χ'' for frequencies as low as 33 Hz at 1.8 K, but there is also a distinct tail at high frequencies indicative of a second relaxation process (Figure S20). This tail becomes less apparent at higher temperatures, and by 2.3 K, it has disappeared. Attempts to use a single modified Debye function could not reproduce these tails and, in general, resulted in unsatisfactory fits to the data. Using CC-FIT,[54] both relaxation processes were fit simultaneously (Figure S21 and Table S10). One of the relaxation processes, τ_1 in Figure S27, appears to be essentially temperature-independent, consistent with quantum tunneling, but no further interpretation of this process is possible since no maximum in χ'' was observed. The second process, τ_2, produces the linear Arrhenius plot shown in Figure S27. This relaxation process is frequency dependent at all measured temperatures, consistent with a thermal relaxation process. The effective barrier extracted for this thermal process is 15 cm^{-1} with a pre-exponential factor of 4.43×10^{-8} s. The alpha values are all less than 0.07, indicating a narrow distribution of relaxation times. The observed barrier is consistent with the one calculated from $(S^2 - 1/4)|D|$ (17 cm^{-1}); the barrier height is also consistent with the energy gap of 2|*D*| (17 cm^{-1}) between the $M_s = \pm^3/_2$ and $M_s = \pm^1/_2$ states, in accord with the relaxation pathway being via an Orbach process.

To further validate the fitting parameters for the thermal process, another fitting of the 400 Oe Cole−Cole data was performed with CC-FIT that did not include the five highest AC frequencies which minimizes the appearance of a tail in the Cole−Cole plot at 1.8 K and virtually eliminates the tail at all higher temperatures. The results of this fitting are shown in Figure S22 and Table S11. The value of U_{eff}/k_b extracted from this fitting is 15 cm^{-1} with $\tau_0 = 2.98 \times 10^{-8}$ s. The alpha values range from 0.12 at 1.8 K to 0.02 at 2.7 K. These results are consistent with the values obtained from the fitting that included two relaxation processes and demonstrate that the tail observed in the Cole−Cole plot is due to a second, fast relaxation process that has little effect on the thermal relaxation mechanism that is observed at high temperatures.

If the DC field is increased to 2000 Oe (Figure 6), then the high-frequency tails are suppressed, and the Cole−Cole plot can be fit with a single relaxation process using CC-FIT (Figure S23 and Table S12) to give U_{eff}/k_b = 16 cm^{-1} and $\tau_0 = 5.28 \times 10^{-8}$ s (Figure 7). The alpha values are now less than 0.22 over the temperature range investigated, slightly higher than the alpha values observed in a 400 Oe DC field. The higher alpha values are likely due to the presence of a minor second relaxation process as can be seen in the very slight tails in the Cole−Cole plot. Attempts to fit the 2000 Oe data with two relaxation processes were unsuccessful. As with the measurements performed in a 400 Oe DC field the observed barrier is consistent with the U_{eff} predicted by $(S^2 - 1/4)|D|$ and the energy gap between M_s states. If the applied DC field is further increased to 2800 Oe, then the AC data become slightly noisy and begin to broaden at higher temperatures, but a good fit can still be obtained (Figures S24, S25, and S28 and Table S13), yielding U_{eff}/k_b = 13 cm^{-1} with $\tau_0 = 5.17 \times 10^{-7}$ s and alpha values of less than 0.36, with the highest temperature having the largest alpha value.

The observed energy barriers are consistent with those expected for an Orbach process (Table 2). For further

DOI: 10.1021/jacs.6b10154
J. Am. Chem. Soc. 2016, 138, 16407−16416

Table 2. Experimental Relaxation Parameters for Compounds 1, 2c, and 3c at Different Applied Fields together with the Experimental *D* Values

compound	field (Oe)	U_{eff}/k_b (cm^{-1})	τ_0 (s)	D (cm^{-1})
1	1000	15.0	1.7×10^{-8}	9.9
	400	15.2	2.98×10^{-8}	
2c	2000	16.4	5.28×10^{-8}	8.7
	2800	13.2	5.17×10^{-7}	
3c	1600	12.3	8.06×10^{-8}	7.4

verification that the Orbach pathway is the principal one, a fit including tunneling, direct, and Raman processes in addition to an Orbach process was performed (eq S2, Figures S30–S32, and Table S15) in the same manner as for compound **1**. For all the fields, the Orbach process is the prevailing one, although at 400 Oe there is a small contribution from tunneling at low temperatures and at 2800 Oe there is a noticeable contribution from the direct process at low temperature. Including these contributions result in slightly different energy barriers, U_{eff}/k_b = 15 cm^{-1} at 400 Oe, U_{eff}/k_b = 18 cm^{-1} at 2000 Oe, and U_{eff}/k_b = 18 cm^{-1} at 2800 Oe. These barriers are consistent with the expected value of 17 cm^{-1}.

Compound **3c** was only investigated in an applied field of 1600 Oe (Figure 6). There are slight tails in the Cole–Cole plot, but fitting the data with two relaxation processes was unsuccessful. Using a single relaxation process (Figure S26 and Table S14), an Arrhenius plot was constructed that gives U_{eff}/k_b = 12 cm^{-1} with $\tau_0 = 8.06 \times 10^{-8}$ s (Figure 7). The alpha values are less than 0.30, and the larger values are likely due to the presence of a second relaxation process, although the magnitude of the observed barrier is consistent with an Orbach relaxation mechanism. The fit including tunneling, direct, and Raman processes (eq S2, Figure S33, and Table S15) shows a contribution from tunneling at lower temperatures and a predominance of an Orbach process at higher temperatures with an energy barrier of U_{eff}/k_b = 20 cm^{-1}, still consistent with thermal relaxation although slightly larger than the expected value of 15 cm^{-1}. One possible explanation for the different values obtained is an overestimation of the tunneling contribution in the fit of the dependence of the relaxation time with field.

In addition, attempts to fit the dependence of τ^{-1} with temperature using only Raman and tunneling were performed for all the compounds, but the fits produced unrealistic values for the Raman process with exponents larger than 9 and pre-exponential factors between 0.2 and 2. Clearly the Raman process is not a major contributor to the relaxation for this family of compounds.

Theoretical Calculations. To further understand the different behavior among the members of this family of trigonal bipyramidal Co^{II} compounds, theoretical calculations using the experimental geometries were performed with Orca 3.0.3 (see Supporting Information for details).[55] ZFS parameters at the CASSCF level are listed in Table 1 together with the experimental values obtained from the fit of the reduced magnetization. For compounds **2t**, **3t**, and **4**, more than one molecule is present in the asymmetric unit; therefore for comparison purposes, the average value is included in Table 1. The values for the different molecules and the values obtained at the NEVPT2 level are provided in Table S16. It can be seen that the calculations correctly reproduce the sign of the *D* value, which is positive only for compound **1**. For the cubic phases, the *E* value is zero as expected due the symmetry of the molecule. When comparing the cubic phases with their analogous triclinic phases, the *D* value is slightly smaller for the three different molecules in the triclinic phase, and the *E* value is nonzero, due to the loss of symmetry and the less than rigorous C_3 axis trough the molecule (Table S16).

For a mononuclear Co^{II} compound in a trigonal bipyramidal geometry, the expected splitting of the d orbitals is shown in Figure 4. The sign and value of *D* is rationalized using the spin–orbit operator, which couples the ground and excited states.

$$\hat{H}_{SO} = \sum_i \xi_i \left(\hat{l}_{Zi} \cdot \hat{s}_{Zi} + \frac{1}{2} (\hat{l}_{+i} \cdot \hat{s}_{-i} + \hat{l}_{-i} \cdot \hat{s}_{+i}) \right) \quad (1)$$

When the excited state results from the excitation between orbitals with the same $|m_l|$ values, the $\Sigma_i \hat{l}_{Zi} \cdot \hat{s}_{Zi}$ operator couples the two orbitals, stabilizing the $M_S = \pm^3/_2$ components and giving rise to a negative contribution to the *D* value. When the excited state results from excitation between orbitals with $|\Delta m_l| = 1$, the $\frac{1}{2} \sum_i \hat{l}_{+i} \cdot \hat{s}_{-i} + \hat{l}_{-i} \cdot \hat{s}_{+i}$ operator is the one that couples the two orbitals, thereby stabilizing the $M_s = \pm^1/_2$ components which leads to a positive contribution to the *D* value.

For the configuration depicted in Figure 4, the first excitation should involve orbitals with different m_l values and hence a positive *D* value, but as demonstrated by Ruamps et al. for the $[Co(Me_6tren)X]^+$ compounds, their ground and excited states are highly multiconfigurational in character.[4] Due to the different determinants that compose the ground and excited states, the $M_s = \pm^3/_2$ level is stabilized when the ground and first excited states couple; the $M_s = \pm^1/_2$ component is stabilized when ground and third or fourth excited states couple. These facts lead to an overall negative *D* value for the $[Co(Me_6tren)X]^+$ compounds.

The difference in the sign of *D* for the acetonitrile compound versus the halide congeners has been analyzed by evaluating the contributions to the *D* value from the different excited states. Table 3 lists the values for compounds **1** and **2c** as well as the value for one of the three different molecules found in **2t**.

The corresponding values for the other molecules in **2t**, **3c** (similar to **2c**), **3t**, and **4** (similar to **2t**) are provided on Table

Table 3. Calculated Energies (cm^{-1}) and Contributions to *D* and *E* values from the First Four Excited States

compound	state	energy	contrib. *D*	contrib. *E*
1	1st ES	3635	−16.5	0.58
	2nd ES	4730	0.70	−0.58
	3rd ES	5383	11.0	11.7
	4th ES	5660	10.8	−10.8
2c	1st ES	3348	−31.9	0
	2nd ES	5040	11.0	−10.5
	3rd ES	5040	11.0	10.5
	4th ES	5516	0	0
2t	1st ES	3345	−30.9	0
	2nd ES	5034	9.60	−8.24
	3rd ES	5235	9.28	6.04
	4th ES	5575	2.69	1.63

DOI: 10.1021/jacs.6b10154
J. Am. Chem. Soc. 2016, 138, 16407–16416

S17. The energy difference between states is very similar for all the compounds. The energy difference between the ground and first excited state is in the range of 3300 to 3700 cm^{-1}, and the next three excited states have energies in the range of 4700 to 5700 cm^{-1}. For the compounds in the cubic phases, the second and third excited states are degenerate. For the triclinic phases, however, the second and third excited states are no longer degenerate. In the case of **1**, the third and fourth excited states are the ones with the largest positive contributions to the *D* value. Although the global *D* value in **1** is positive, the contribution from the first excited state is still negative as observed for the halide congeners. This negative contribution, however, is smaller than that for the halide analogues, whereas the positive contributions from the other excited states are of similar magnitude for all the complexes. Consequently, a global positive *D* value for **1** and negative *D* values for the halide series of compounds are observed. The energies of the different excited states are very similar for all of the compounds, which does not explain the smaller negative contribution to the *D* value in **1**. The smaller contribution may be due to the multiconfigurational character of the wave function and the different weight of the determinants that compose the ground state in **1** in comparison with the other compounds (Figure S34 and Table S18).

Magneto-Structural Correlations. If one considers only the halide series of compounds, then it is reasonable to attribute the SMM behavior of the cubic phases to the presence of strict 3-fold symmetry and the lack thereof in the triclinic phases. This symmetry argument, however, does not explain the SMM behavior of the acetonitrile complex. The bonding metrics support a similar electronic structure for all members of the family. The bond distances between the Co^{II} ion and the atom coordinated to the open site left by TPMA ligand follow a reasonable trend, *viz.*, a lengthening from CH_3CN to iodide. The projection of the Co^{II} ion out of the equatorial N3 plane is similar for all of the members of the family, as are the distances and angles between the Co^{II} ion and the TPMA ligand (Table S2). What is different, however, is the nearest-neighbor distances between cobalt ions. For **2t**, **3t**, and **4**, in which SMM behavior is not observed, the shortest Co···Co distance is in the range of 6.119 to 6.601 Å. For **1**, **2c**, and **3c** the shortest Co···Co intermolecular distance is in the range of 7.863 to 8.079 Å, much longer than that in the triclinic halide phases. These increased cobalt distances, taken together with the narrow distribution of distances for the analogs that display similar SMM behavior, strongly suggest that dipolar interactions are the source of fast relaxation in the members of the family that do not display SMM behavior. In the $[Co(Me_6tren)Cl]ClO_4$ and $[Co(Me_6tren)Br]Br$ complexes[4] the closest Co···Co contact is 7.95 Å for the chloride complex and 8.155 Å for the bromide complex, similar to the Co···Co distances in this study. No AC susceptibility experiments were performed in that report, making a direct comparison of the SMM properties to the ones in this study impossible, but micro-SQUID measurements displayed open hysteresis loops below 1 K, thus confirming the SMM behavior of the Me_6tren complexes. A dilution study with Co/Zn ratios of 0.1:0.9 and 0.05:0.95 revealed that dipolar interactions are not important for the relaxation, lending support to the hypothesis that Co···Co contacts of ∼8 Å are sufficient to suppress dipolar relaxation. Recently, the AC magnetic behavior of $[Co(Me_6tren)Cl](ClO_4)$ was reported.[56] This compound displayed weak out-of-phase signals in a zero applied DC field and a spin reversal barrier of ∼20 K across a range of applied DC fields from 2000 to 8000 Oe. This behavior is remarkably similar to the properties of the cubic phase of [Co(TPMA)Cl]Cl. In the case of $[Co(Me_6tren)H_2O](NO_3)_2$, the closest Co···Co contact is 7.791 Å,[5] but no maximum in χ'' was observed at 1.9 K, even at DC fields as high as 7000 Oe, consistent with a very fast relaxation mechanism. No investigation of the mechanism of the fast relaxation was reported. This Co···Co distance is only 0.072 Å shorter than that observed for **1**, which is the SMM with the shortest Co···Co distance in this study. One may argue that since the magnitude of the dipolar interaction scales as r^{-3} that the small difference in intermolecular distance is responsible for the changes in magnetic behavior, but this scenario is unlikely. It has recently been shown that the interaction between the electron spin and the nuclear spin of cobalt can also have a significant impact on the relaxation properties in these types of systems,[53] as can vibronic coupling.[57] In the absence of further experimental and theoretical studies, the presence of the water protons in $[Co(Me_6tren)H_2O](NO_3)_2$ leading to an increase in vibronic coupling is a more viable explanation for the much faster relaxation observed in $[Co(Me_6tren)H_2O](NO_3)_2$ as compared to $[Co(Me_6tren)Cl](ClO_4)$, $[Co(Me_6tren)Br]Br$, and $[Co(TPMA)X]^+$ complexes described in this work. Also, the coordinated water molecule forms hydrogen bonds to the nitrate counteranions in that molecule. There are no classic hydrogen bonds, however, between the coordinated CH_3CN molecule and the tetrafluoroborate counteranions in $[Co(TPMA)CH_3CN](BF_4)_2$.

In the case of other ligands such as tbta (tbta = tris[(1-benzyl-1H-1,2,3-triazol-4-yl)methyl]amine) and NS_3^{iPr}, the comparison is more complex due to the different nature and sizes of the ligand. Both complexes exhibit SMM behavior with their shortest Co···Co intermolecular distances being longer than 8 Å. In the case of $[Co(NS_3^{iPr})Cl](BPh_4)$,[27] AC susceptibility data (under an applied DC field) and micro-SQUID measurements were reported; the shortest Co···Co intermolecular distance is 8.518 Å. For $[Co(tbta)N_3](ClO_4)\cdot 3CH_3CN$,[26] the shortest Co···Co distance is 8.186 Å, and the molecule exhibits an energy barrier close to 2D under an applied field of 3000 Oe.

The greater flexibility of the Me_6tren ligand as compared to that of TPMA may also be responsible for the differences in magnetic behavior but it is not likely to be a major influence given the similarity in the AC magnetic behavior of $[Co(Me_6tren)Cl](ClO_4)$ and **2c**. Transverse magnetic fields caused by the internal field of neighboring molecules have been shown to increase the tunneling probability in SMMs.[58] All of the members of this series display less than ideal packing arrangements in this respect. Figure 8 displays schematic packing diagrams of the different members of the series as viewed down the crystallographic *c* axis. As can be seen in Figure 8, the C_3 axes of neighboring molecules are not colinear for any of these molecules. The transverse dipolar fields generated by these packing arrangements promote quantum tunneling, explaining why a DC field is needed to observe SMM behavior even in the cubic analogs **2c** and **3c**, in which *E* is vanishingly small.

■ CONCLUSIONS

Experimental and computational studies were performed on a new family of mononuclear Co^{II} compounds with the TPMA ligand, which enforces trigonal bipyramidal geometry. Different

DOI: 10.1021/jacs.6b10154
J. Am. Chem. Soc. 2016, 138, 16407−16416

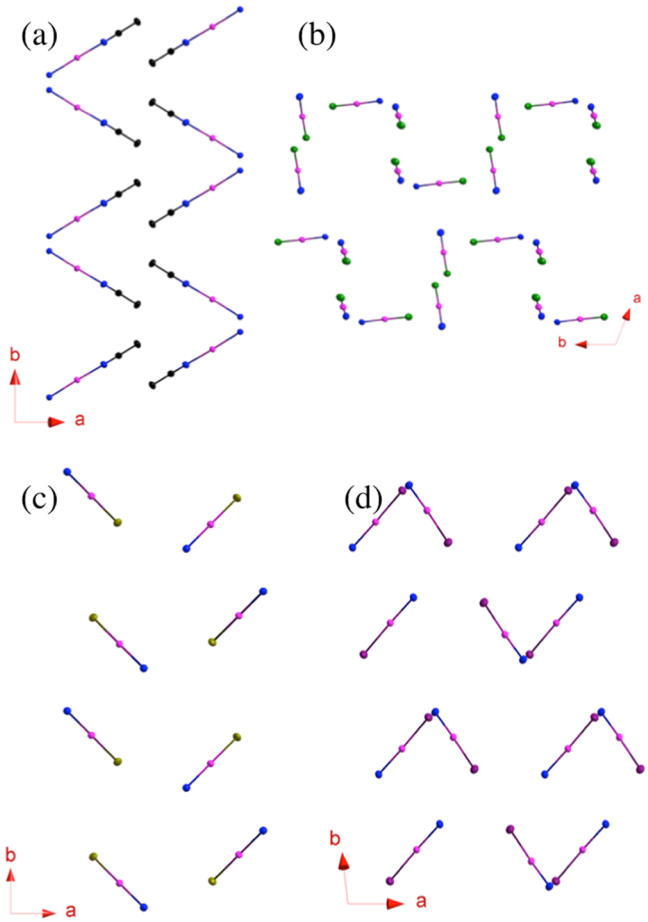

Figure 8. Packing arrangement of members of the $[Co(TPMA)X]^{n+}$ family. Only the atoms defining the C_3 axes are shown for the sake of clarity. (a) **1**. (b) **2t**. The triclinic phase of **3t** is identical. (c) **3c**. The cubic phase of **2c** is identical. (d) **4**. Color code: C, black; N, blue; Co, pink; Cl, green; Br, yellow; I, purple.

axial ligands were explored with the CH_3CN derivative, **1**, which exhibits a positive *D* value, and the halide congeners that exhibit negative *D* values. All of the compounds have a very strong multiconfigurational character of the wave function. The positive *D* value observed for **1** arises from the smaller negative contribution of the first excited state to the *D* value. Compounds **1**, **2c**, and **3c** display SMM behavior with a dependence of the relaxation time on temperature that follows Arrhenius behavior and leads to energy barriers expected for an Orbach relaxation process, confirming that no other relaxation processes are predominant for these complexes. The absence of SMM behavior for **2t**, **3t**, and **4** is attributed to the shorter intermolecular Co···Co separations, which allow for stronger dipolar interactions and hence faster spin relaxation. These studies provide further evidence of the effects of small perturbations on magnetic relaxation pathways in SMMs, and the information unveiled contributes to a more in-depth understanding of relaxation pathways, the ultimate goal of which is to improve the deliberate tailoring of magnetic molecules.

■ ASSOCIATED CONTENT

Supporting Information

The Supporting Information is available free of charge on the acS Publications website at DOI: 10.1021/jacs.6b10154.

Experimental details, powder diffraction patterns, thermograms, reduce magnetization measurements, ac susceptibility measurements, fits of the dependence of the relaxation time with field and temperature including several relaxation processes, and computational details (PDF)

Crystal structures of compounds **1**−**4** (CIF)

■ AUTHOR INFORMATION

Corresponding Author

*E-mail: dunbar@chem.tamu.edu.

ORCID

Toby J. Woods: 0000-0002-1737-811X

María F. Ballesteros-Rivas: 0000-0001-9497-0339

Silvia Gómez-Coca: 0000-0002-2299-4697

Eliseo Ruiz: 0000-0001-9097-8499

Kim R. Dunbar: 0000-0001-5728-7805

Present Addresses

§School of Chemical Sciences, University of Illinois at Urbana-Champaign, Urbana, IL 61801, United States.

⊥Centro Conjunto de Investigacion en Quimica Sustentable UAE Mex-UNAM (CCIQS), Carretera Toluca-Altacomulco, km 14.5, Toluca, Estado de Mexico, C.P. 50200, Mexico.

∥Department of Chemistry, King's College London, London SE1 1DB, United Kingdom.

Author Contributions

T.J.W. and M.F.B.-R. contributed equally to the creation of this work.

Notes

The authors declare no competing financial interest.

■ ACKNOWLEDGMENTS

The work performed at TAMU was supported the U.S. Department of Energy, Basic Energy Sciences, Materials Sciences Division under Grant DE-SC0012582. K.R.D. gratefully acknowledges the Robert A. Welch Foundation for financial support (A-1449). T.J.W. thanks the Department of Energy Office of Science Graduate Fellowship Program (DOE SCGF), made possible in part by the American Recovery and Reinvestment Act of 2009, administered by ORISE-ORAU under contract No. DE-ac05-06OR23100, for fellowship support. M.F.B.-R. thanks the Instituto de Ciencia y Tecnología del Distrito Federal (ICyTDF) for fellowship support. E.R. thanks the Spanish Ministerio de Economía y Competitividad (MINECO) (grant CTQ2015-64579-C3-1-P, FEDER/EU), Generalitat de Catalunya for an ICREA Academia award and CSUC for computational resources.

■ REFERENCES

(1) Aravena, D.; Ruiz, E. *Inorg. Chem.* **2013**, *52*, 13770.

(2) Sorace, L.; Benelli, C.; Gatteschi, D. *Chem. Soc. Rev.* **2011**, *40*, 3092.

(3) Woodruff, D. N.; Winpenny, R. E. P.; Layfield, R. A. *Chem. Rev.* **2013**, *113*, 5110.

(4) Ruamps, R.; Batchelor, L. J.; Guillot, R.; Zakhia, G.; Barra, A.-L.; Wernsdorfer, W.; Guihery, N.; Mallah, T. *Chem. Sci.* **2014**, *5*, 3418.

(5) Pinero Cruz, D. M.; Woodruff, D. N.; Jeon, I.-R.; Bhowmick, I.; Secu, M.; Hillard, E. A.; Dechambenoit, P.; Clerac, R. *New J. Chem.* **2014**, *38*, 3443.

(6) Karasawa, S.; Nakano, K.; Yoshihara, D.; Yamamoto, N.; Tanokashira, J.-i.; Yoshizaki, T.; Inagaki, Y.; Koga, N. *Inorg. Chem.* **2014**, *53*, 5447.

(7) Herchel, R.; Váhovská, L.; Potočňák, I.; Trávníček, Z. *Inorg. Chem.* **2014**, *53*, 5896.
(8) Eichhöfer, A.; Lan, Y.; Mereacre, V.; Bodenstein, T.; Weigend, F. *Inorg. Chem.* **2014**, *53*, 1962.
(9) Boča, R.; Miklovič, J.; Titiš, J. *Inorg. Chem.* **2014**, *53*, 2367.
(10) Bar, A. K.; Pichon, C.; Sutter, J.-P. *Coord. Chem. Rev.* **2016**, *308*, 346.
(11) Gómez-Coca, S.; Aravena, D.; Morales, R.; Ruiz, E. *Coord. Chem. Rev.* **2015**, *289*−*290*, 379.
(12) Craig, G. A.; Murrie, M. *Chem. Soc. Rev.* **2015**, *44*, 2135.
(13) Frost, J. M.; Harriman, K. L. M.; Murugesu, M. *Chem. Sci.* **2016**, *7*, 2470.
(14) Zadrozny, J. M.; Xiao, D. J.; Atanasov, M.; Long, G. J.; Grandjean, F.; Neese, F.; Long, J. R. *Nat. Chem.* **2013**, *5*, 577.
(15) Zadrozny, J. M.; Atanasov, M.; Bryan, A. M.; Lin, C.-Y.; Rekken, B. D.; Power, P. P.; Neese, F.; Long, J. R. *Chem. Sci.* **2013**, *4*, 125.
(16) Mossin, S.; Tran, B. L.; Adhikari, D.; Pink, M.; Heinemann, F. W.; Sutter, J.; Szilagyi, R. K.; Meyer, K.; Mindiola, D. J. *J. Am. Chem. Soc.* **2012**, *134*, 13651.
(17) Poulten, R. C.; Page, M. J.; Algarra, A. G.; et al. *J. Am. Chem. Soc.* **2013**, *135*, 13640.
(18) Lin, W.; Bodenstein, T.; Mereacre, V.; Fink, K.; Eichhöfer, A. *Inorg. Chem.* **2016**, *55*, 2091.
(19) Miklovič, J.; Valigura, D.; Boča, R.; Titiš, J. *Dalton Trans.* **2015**, *44*, 12484.
(20) Huang, X.-C.; Zhou, C.; Shao, D.; Wang, X.-Y. *Inorg. Chem.* **2014**, *53*, 12671.
(21) Chen, L.; Wang, J.; Wei, J.-M.; Wernsdorfer, W.; Chen, X.-T.; Zhang, Y.-Q.; Song, Y.; Xue, Z.-L. *J. Am. Chem. Soc.* **2014**, *136*, 12213.
(22) Rechkemmer, Y.; Breitgoff, F. D.; van der Meer, M.; Atanasov, M.; Hakl, M.; Orlita, M.; Neugebauer, P.; Neese, F.; Sarkar, B.; van Slageren, J. *Nat. Commun.* **2016**, *7*, 10467.
(23) Nemec, I.; Marx, R.; Herchel, R.; Neugebauer, P.; van Slageren, J.; Trávníček, Z. *Dalton Trans.* **2015**, *44*, 15014.
(24) Nemec, I.; Liu, H.; Herchel, R.; Zhang, X.; Trávníček, Z. *Synth. Met.* **2016**, *215*, 158.
(25) Nemec, I.; Herchel, R.; Trávníček, Z. *Dalton Trans.* **2016**, *45*, 12479.
(26) Schweinfurth, D.; Sommer, M. G.; Atanasov, M.; Demeshko, S.; Hohloch, S.; Meyer, F.; Neese, F.; Sarkar, B. *J. Am. Chem. Soc.* **2015**, *137*, 1993.
(27) Shao, F.; Cahier, B.; Guihéry, N.; et al. *Chem. Commun.* **2015**, *51*, 16475.
(28) Tyeklar, Z.; Jacobson, R. R.; Wei, N.; Murthy, N. N.; Zubieta, J.; Karlin, K. D. *J. Am. Chem. Soc.* **1993**, *115*, 2677.
(29) Heintz, R. A.; Smith, J. A.; Szalay, P. S.; Weisgerber, A.; Dunbar, K. R. *Inorg. Synth.* **2002**, *33*, 75.
(30) Chan, S. L.-F.; Lam, T. L.; Yang, C.; Yan, S.-C.; Cheng, N. M. *Chem. Commun.* **2015**, *51*, 7799.
(31) *APEX2*, v2013.10−0; Bruker AXS: Madison, WI, 2013.
(32) Sheldrick, G. M. *Acta Crystallogr., Sect. A: Found. Crystallogr.* **2008**, *64*, 112.
(33) Sheldrick, G. *Acta Crystallogr., Sect. A: Found. Adv.* **2015**, *71*, 3.
(34) Hubschle, C. B.; Sheldrick, G. M.; Dittrich, B. *J. Appl. Crystallogr.* **2011**, *44*, 1281.
(35) Alvarez, S.; Alemany, P.; Casanova, D.; Cirera, J.; Llunell, M.; Avnir, D. *Coord. Chem. Rev.* **2005**, *249*, 1693.
(36) *Shape*, version 2.0; Universitat de Barcelona: Barcelona, Spain, 2010.
(37) Chilton, N. F.; Anderson, R. P.; Turner, L. D.; Soncini, A.; Murray, K. S. *J. Comput. Chem.* **2013**, *34*, 1164.
(38) Cole, K. S.; Cole, R. H. *J. Chem. Phys.* **1941**, *9*, 341.
(39) Aubin, S. M. J.; Sun, Z.; Pardi, L.; Krzystek, J.; Folting, K.; Brunel, L.-C.; Rheingold, A. L.; Christou, G.; Hendrickson, D. N. *Inorg. Chem.* **1999**, *38*, 5329.
(40) Zhu, Y.-Y.; Cui, C.; Zhang, Y.-Q.; et al. *Chem. Sci.* **2013**, *4*, 1802.
(41) Zadrozny, J. M.; Telser, J.; Long, J. R. *Polyhedron* **2013**, *64*, 209.
(42) Huang, W.; Liu, T.; Wu, D.; Cheng, J.; Ouyang, Z. W.; Duan, C. *Dalton Trans.* **2013**, *42*, 15326.
(43) Habib, F.; Luca, O. R.; Vieru, V.; et al. *Angew. Chem., Int. Ed.* **2013**, *52*, 11290.
(44) Zadrozny, J. M.; Liu, J.; Piro, N. A.; Chang, C. J.; Hill, S.; Long, J. R. *Chem. Commun.* **2012**, *48*, 3927.
(45) Karasawa, S.; Nakano, K.; Tanokashira, J.-i.; Yamamoto, N.; Yoshizaki, T.; Koga, N. *Dalton Trans.* **2012**, *41*, 13656.
(46) Buchholz, A.; Eseola, A. O.; Plass, W. *C. R. Chim.* **2012**, *15*, 929.
(47) Zadrozny, J. M.; Long, J. R. *J. Am. Chem. Soc.* **2011**, *133*, 20732.
(48) Yoshihara, D.; Karasawa, S.; Koga, N. *Polyhedron* **2011**, *30*, 3211.
(49) Karasawa, S.; Koga, N. *Inorg. Chem.* **2011**, *50*, 5186.
(50) Jurca, T.; Farghal, A.; Lin, P.-H.; Korobkov, I.; Murugesu, M.; Richeson, D. S. *J. Am. Chem. Soc.* **2011**, *133*, 15814.
(51) Vallejo, J.; Castro, I.; Ruiz-García, R.; Cano, J.; Julve, M.; Lloret, F.; De Munno, G.; Wernsdorfer, W.; Pardo, E. *J. Am. Chem. Soc.* **2012**, *134*, 15704.
(52) Wu, D.; Zhang, X.; Huang, P.; Huang, W.; Ruan, M.; Ouyang, Z. W. *Inorg. Chem.* **2013**, *52*, 10976.
(53) Gómez-Coca, S.; Urtizberea, A.; Cremades, E.; Alonso, P. J.; Camón, A.; Ruiz, E.; Luis, F. *Nat. Commun.* **2014**, *5*, 4300.
(54) Chilton, N. F. *CC-FIT*; Manchester, U.K., 2014. http://www.nfchilton.com/cc-fit.html.
(55) Neese, F. *WIREs Comput. Mol. Sci.* **2012**, *2*, 73.
(56) Packová, A.; Miklovič, J.; Boča, R. *Polyhedron* **2015**, *102*, 88.
(57) Atanasov, M.; Zadrozny, J. M.; Long, J. R.; Neese, F. *Chem. Sci.* **2013**, *4*, 139.
(58) Glaser, T.; Hoeke, V.; Gieb, K.; Schnack, J.; Schröder, C.; Müller, P. *Coord. Chem. Rev.* **2015**, *289*−*290*, 261.

DOI: 10.1021/jacs.6b10154
J. Am. Chem. Soc. 2016, 138, 16407−16416